ACS Photonics

Article

Cite This: ACS Photonics 2019, 6, 2530−2536

pubs.acs.org/journal/apchd5

Observation of Enhanced Optical Spin Hall Effect in a Vertical Hyperbolic Metamaterial

Minkyung Kim,[†,‡] Dasol Lee,[†,‡] Tae Hak Kim,[§] Younghwan Yang,[†] Hui Joon Park,[§] and Junsuk Rho*[,†,⊥]

[†]Department of Mechanical Engineering, Pohang University of Science and Technology (POSTECH), Pohang 37673, Republic of Korea

[§]Department of Organic and Nano Engineering, Hanyang University, Seoul 04763, Korea

[⊥]Department of Chemical Engineering, Pohang University of Science and Technology (POSTECH), Pohang 37673, Republic of Korea

Supporting Information

ABSTRACT: Hyperbolic metamaterials, horizontally stacked metal and dielectric multilayer, have recently been studied as a platform to observe optical spin Hall effect. However, the large optical spin Hall effect in the horizontal hyperbolic metamaterials accompanies extremely low transmission, which obstructs its practical applications. Reducing the sample thickness to augment the transmission causes diminishment of the optical spin Hall effect. In this Article, we demonstrate that a vertical hyperbolic metamaterial can enhance the optical spin Hall effect by several orders of magnitude in comparison to that of its horizontal counterpart. Under the same conditions of material combinations and total thickness, the enhancement, which is incident angle-dependent, can be higher than 800-fold when the incident angle is 5° and 5000-fold when the incident angle is 1°. As a proof of concept, we fabricate a large-scale gold nanograting by nanoimprint lithography and observe the optical spin Hall effect experimentally, which agrees well with the simulated result. The gigantic optical spin Hall effect in a vertical hyperbolic metamaterial will enable helicity-dependent control of optical devices including filters, sensors, switches, and beam splitters.

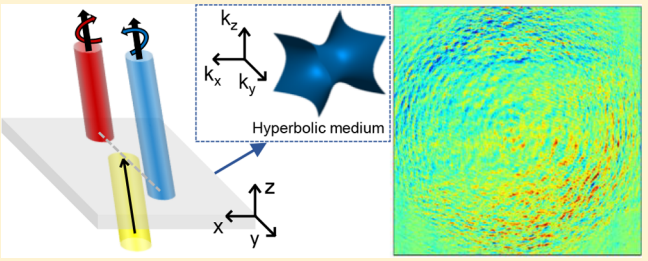

KEYWORDS: *photonic spin Hall effect, spin Hall effect of light, hyperbolic metamaterials, hyperbolic metasurface, nanoimprint lithography, Stokes polarimetry setup*

Hyperbolic metamaterials are artificially structured materials that are designed to exhibit a hyperbolic shape of equi-frequency contour. Highly anisotropic electric responses of the hyperbolic metamaterials, represented as opposite signs of permittivities along direction, have shown potential in a variety of applications such as super-resolution imaging,[1−4] enhancement of spontaneous emission,[5] and anomalous scaling laws.[6] Among the many applications of hyperbolic metamaterials, optical spin Hall effect (OSHE), an optical counterpart of the spin Hall effect, has received growing attention recently.[7−9] OSHE, which refers to the spin-dependent transverse splitting of linearly polarized incidence,[10−12] can be facilitated by the extreme anisotropic properties of the hyperbolic metamaterials, even with a sample thinner than a wavelength. OSHE in hyperbolic metamaterials has been recently reported theoretically[7,8] and experimentally[9] by horizontally stacking metal and dielectric multilayer alternately, parallel to the normal vector of the substrate; this structure will be referred to as a horizontal hyperbolic metamaterial (hHMM). However, the enhanced OSHE in hHMMs accompanies extremely low efficiency below 0.01, inhibiting practical applications. This drawback can be overcome by an alternative arrangement that is a vertical hyperbolic metamaterial (vHMM) in which interfaces between dielectric and metal are perpendicular to the normal vector of the substrate.

Here we present several orders of magnitude enhancement of OSHE compared to that in hHMMs using a vHMM. Despite the advantages of vHMMs over hHMMs in many applications such as super-resolution imaging[13] and broadband negative refraction due to the nonresonant characteristics, OSHE using vHMM has not been studied yet. We demonstrate numerically that the different optic axis configurations in vHMMs increase the difference between the transmission coefficients of s- and p-polarization, thereby giving rise to a significant enhancement of the OSHE. Then, the enhanced OSHE is experimentally verified by a Stokes polarimetry method.

Received: June 24, 2019
Published: September 9, 2019

DOI: 10.1021/acsphotonics.9b00904
ACS Photonics 2019, 6, 2530−2536

RESULTS AND DISCUSSION

The underlying principle of OSHE is angular momentum conservation, which leads to spin−orbit coupling. For intuitive understanding, we imagine an incident Gaussian beam propagating in the x−z plane (Figure 1a). Ideally, the transmitted beam should also be in the x−z plane. However, a Gaussian beam with a finite thickness includes noncentral wave vectors $\mathbf{k}_c + d\mathbf{k}$, where $\mathbf{k}_c$ is a central wave vector. The deflection $d\mathbf{k}$ can be either in-plane ($dk_{\parallel}$) or out-of-plane ($dk_{\perp}$), which results in a discrepancy of incident angle and incident plane, respectively (Figure 1b). Considering that the p- and s-polarizations are defined with respect to the wave vector, the deflection in momentum space (extrinsic orbital angular momentum) also alters the basis of polarization (spin angular momentum) and induces a spin-dependent Berry phase.[14] Therefore, a linearly polarized incidence, which can be regarded as a superposition of left/right-circularly polarized light (LCP/RCP), is split along the y-axis by an amount of the transverse shift δ into two circularly polarized beams with the oppositely shifted beam centroids (Figure 1a).

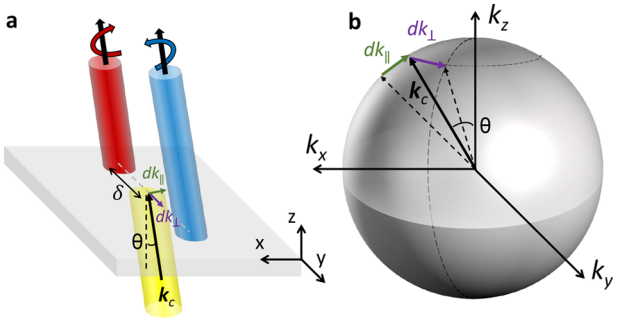

Figure 1. Schematics of optical spin Hall effect in (a) real space and (b) momentum space. (a) Incident Gaussian beam with a finite thickness containing noncentral wave vectors. Black solid line denotes central wave vector $\mathbf{k}_c$. Green and purple lines represent in-plane ($dk_{\parallel}$) and out-of-plane ($dk_{\perp}$) deflection, respectively. The transverse shift is denoted as δ. (b) A sphere in momentum space with in-plane ($dk_{\parallel}$) and out-of-plane ($dk_{\perp}$) deflections. The shift and deflections are exaggerated for better visualization.

δ is usually limited to a fraction of wavelength, as a result of the weak spin−orbit coupling, and is difficult to observe experimentally. Therefore, observation of the small δ requires amplification of the signal by using quantum weak measurements involving preselection and postselection techniques.[15,16] Alternatively, δ can be enhanced by exploiting recent advances in metamaterials. Enhancement of OSHE based on metamaterials has been demonstrated during the past several years using metasurfaces,[12] epsilon-near-zero metamaterial[17] and hyperbolic metamaterials.[7−9] Although hHMMs have shown a huge δ of up to a few tens of micrometers[7,8] and even beyond[9] in the visible range, they suffer from extremely low transmittance below 0.01, which hinders practical applications. The low efficiency can be overcome by decreasing the thickness, but this change also reduces δ.

We propose a deep-subwavelength thin vHMM, which exhibits a gigantic OSHE with high efficiency, to solve this issue. The optic axis of a vHMM is perpendicular to the normal vector of the substrate, whereas the optic axis of a hHMM is parallel to it. This different configuration enables the enhancement of δ with high efficiency. Recently, the OSHE of a beam reflected by black phosphorus, an anisotropic two-dimensional atomic crystal, has been numerically reported.[18] It demonstrates the possibility of large OSHE in an atomically thin sample, but δ barely exceeds one wavelength. To enhance the OSHE, we examine the analytic formula of δ. When a

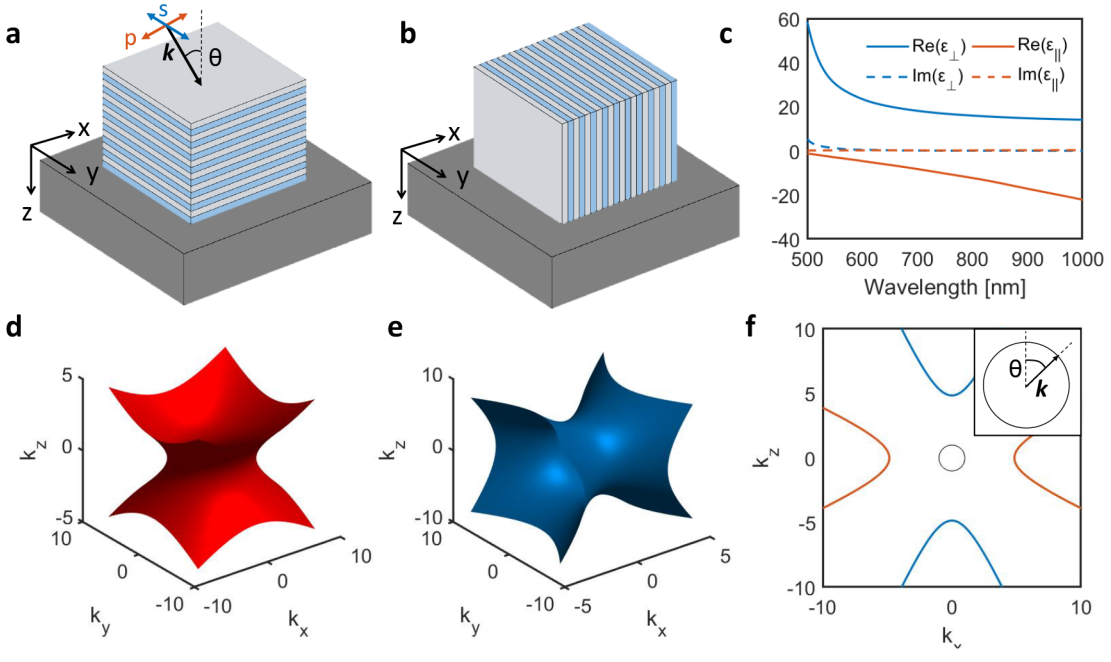

Figure 2. Schematics of (a) hHMM and (b) vHMM. In a hHMM (vHMM), metal and dielectric interfaces are parallel (perpendicular) to the propagation direction of normal incidence. Incident plane is x−z plane and z-axis is the normal in the schematics. (c) Effective permittivities of Ag and TiO_2 multilayer with equal volume fraction. Equifrequency contour of a (d) hHMM and (e) vHMM consisting of Ag and TiO_2. (f) Equifrequency curve of the hHMM (red) and vHMM (blue) in the k_x−k_z plane. Black curve represents the equifrequency curve of air. Inset shows a magnified image of the light cone.

DOI: 10.1021/acsphotonics.9b00904
ACS Photonics 2019, 6, 2530−2536

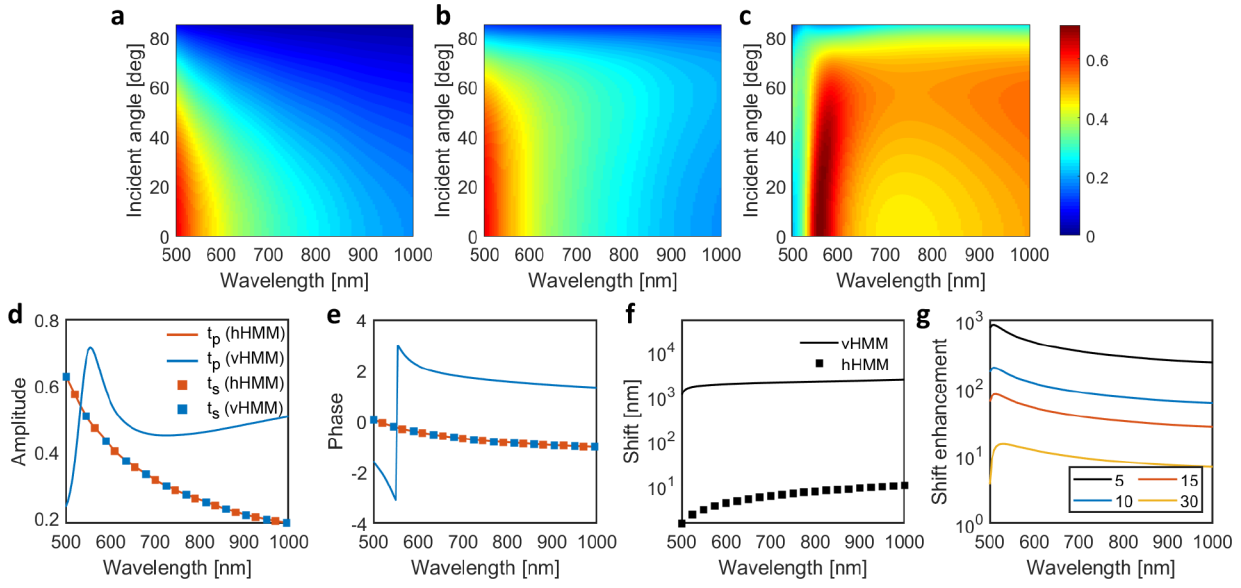

Figure 3. Amplitude of (a) t_s and (b) t_p of hHMM. (c) Amplitude of t_p of vHMM. (d) Amplitude and (e) phase of transmission coefficients and (f) δ when the incident angle is 5°. (g) Shift enhancement ($\delta_{vHMM}/\delta_{hHMM}$) calculated by eq 2 at four different incident angles.

horizontally polarized beam is injected from medium 1 with a refractive index n_1, δ of the beam transmitted through an anisotropic medium is provided as[7,8]

$$\delta_H^{\pm} = \pm \frac{k_1 w_0^2 \cot\theta_i \left(t_p^2 \frac{\cos\theta_t}{\cos\theta_i} - t_p t_s \right)}{k_1^2 w_0^2 t_p^2 + \cot\theta_i^2 \left(t_p \frac{\cos\theta_t}{\cos\theta_i} - t_s \right)^2 + \left(\frac{\partial t_p}{\partial \theta_i} \right)^2} \quad (1)$$

where $k_1 = n_1 k_0$, where k_0 is the wave vector in free space; + (−) corresponds to LCP (RCP); w_0 is a beam waist; θ_i and θ_t are incident and transmitted angles, respectively t_p and t_s are transmission coefficients of p- and s-polarizations, respectively. When the beam waist is sufficiently large ($k_1^2 w_0^2 \gg \cot^2\theta_i$), the eq 1 can be simplified to[19]

$$\delta_H^{\pm} = \pm \frac{\cot\theta_i}{k_1} \mathrm{Re}\left(1 - \frac{t_s}{t_p} \right) \quad (2)$$

Since δ is proportional to the real part of $1 - t_s/t_p$ and $\cot\theta_i$, a natural way to enhance δ is to either increase the difference between t_s and t_p or to decrease θ_i. To determine why vHMM amplifies OSHE more than hHMM does, we examine the effective parameters of the two cases. According to effective medium theory (EMT), a structure with a deep-subwavelength scale can be approximated by a homogeneous medium with effective parameters. The permittivity of a multilayer-based hyperbolic metamaterial is[20]

$$\varepsilon_{\parallel} = f\varepsilon_m + (1-f)\varepsilon_d$$
$$\varepsilon_{\perp} = \frac{\varepsilon_m \varepsilon_d}{(1-f)\varepsilon_m + f\varepsilon_d} \quad (3)$$

where ε is a relative permittivity, subscripts m and d represent metal and dielectric, respectively, subscripts $\perp$ and $\parallel$ correspond to directions perpendicular and parallel to the interfaces, and f is a metal filling ratio. Permittivity tensor of hHMM is $\varepsilon_{hHMM} = \mathrm{diag}(\varepsilon_{\parallel}, \varepsilon_{\parallel}, \varepsilon_{\perp})$ for hHMM (Figure 2a) and $\varepsilon_{vHMM} = \mathrm{diag}(\varepsilon_{\perp}, \varepsilon_{\parallel}, \varepsilon_{\parallel})$ for vHMM (Figure 2b). s-Polarized incidence, whose electric field has a y-component only, experiences the y-component of permittivity. Since hHMM and vHMM have the same permittivity along y-axis, they have the same t_s. In contrast, p-polarized light has both x- and z-components of the electric field. When incident angle is large ($\theta_i \sim \pi/2$), the p-polarized light experiences the z-component of permittivity dominantly. Then, the difference between t_s and t_p of an hHMM is large but δ remains small due to the cot θ_i term in eq 2. However, when incident angle is small ($\theta_i \ll \pi/2$), the x-component of permittivity is dominant. Therefore, a vHMM exhibits significant discrepancy between t_p and t_s at small incident angle, while they are rather similar in a hHMM. To sum up, a vHMM works as a polarizer, and the polarization-dependent transmission coefficients of vHMMs at small θ_i yield a gigantic OSHE. This EMT-based analysis can be applied to general anisotropic materials, not limited to hyperbolic metamaterials. Therefore, a vertically stacked dielectric multilayer, which possesses an elliptical equi-frequency contour, can also induce higher OSHE compared to their horizontal counterpart. However, due to weak anisotropy in the dielectric multilayer, its OSHE is not as strong as in hyperbolic metamaterials (see comparison between vertically and horizontally stacked dielectric multilayers, Supporting Information).

The enhanced OSHE in vHMM can be also understood by examining an equi-frequency contour. To compare the difference between hHMM and vHMM clearly, we use a multilayer of silver (Ag) and titanium dioxide (TiO_2) with f = 0.5 (Figure 2a.b), which has positive $\varepsilon_{\perp}$ and negative $\varepsilon_{\parallel}$ (Figure 2c). Such a medium with two negative and one positive diagonal element of permittivity tensor exhibits type-II hyperbolic dispersion. Equifrequency contours of hHMM and vHMM at 600 nm are shown in Figure 2d–f. The hyperbolic equifrequency contours correspond to p-polarized modes. On the contrary, the s-polarized modes have purely imaginary equifrequency contours originating from the negative permittivity elements. Therefore, incident light with s-polarization cannot be effectively coupled to the hyperbolic metamaterials. It is also true for p-polarized light incident to hHMM. Considering that the tangential wave vector k_x should be

DOI: 10.1021/acsphotonics.9b00904
ACS Photonics 2019, 6, 2530−2536

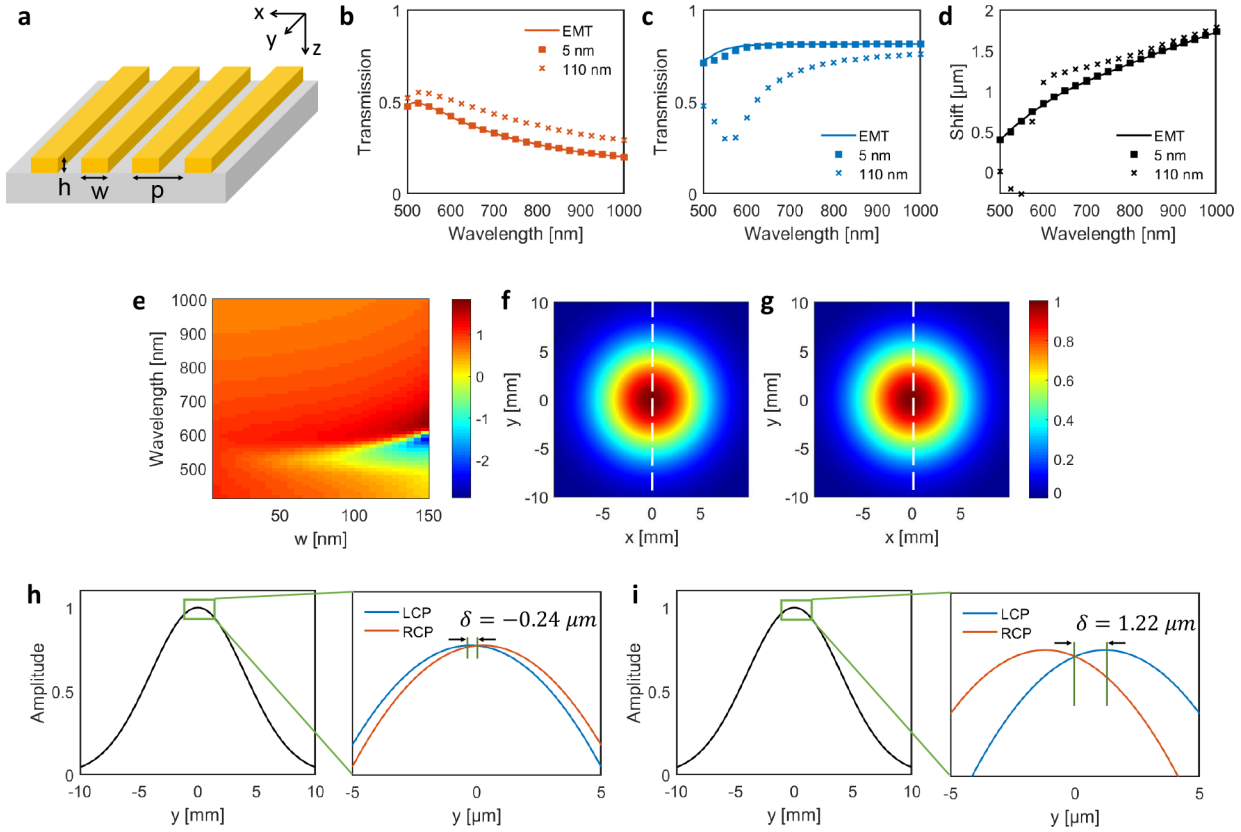

Figure 4. (a) An illustration of a realistic vHMM. Amplitude of (b) t_s and (c) t_p. (d) δ calculated by EMT and realistic structure. (e) δ of the realistic structure divided by δ calculated by EMT. Field profile of (f) left- and (g) right-circularly polarized light at 532 nm. Field amplitude along the white dashed line at (h) 532 nm and (i) 638 nm. Beam waist w_0 is 4 mm and $\theta_i = 5°$.

continuous at the interface, the light cone cannot excite any mode of the hHMM, because p-polarized mode of the hHMM has high k_x-components only (Figure 2f). In contrast, since the optic axis of a vHMM is along the x-axis, the vHMM has p-polarized k_x-components, which overlap those of the light cone. Therefore, p-polarized incidence can couple to vHMM, which gives rise to higher transmission of vHMMs in comparison to hHMMs. Although we use type-II hyperbolic metamaterial throughout the manuscript, the enhancement of the optical spin Hall effect is applicable to both type-I and type-II hyperbolicity (see optical spin Hall effect in a type-I hyperbolic metamaterial, Supporting Information).

In order to quantitatively compare the OSHE of hHMM and vHMM, transmission coefficients of two media are calculated using EMT (see transmission coefficients from effective medium theory, Supporting Information). t_s and t_p of a hHMM consisting of Ag and TiO_2 layers, with a total thickness of d = 50 nm placed on a glass substrate, are shown in Figure 3a,b. Because t_s of vHMM is the same as for the hHMM, only t_p of a vHMM composed of the same materials and total thickness is shown in Figure 3c. Difference of t_s and t_p is noticeable in the vHMM, while they are unremarked in the hHMM especially at small θ_i. To emphasize the difference, transmission coefficients and δ when $\theta_i = 5°$ are plotted in Figure 3d–f. The hHMM supports indistinguishable t_s and t_p, which leads to δ of only a few nanometers. In contrast, the vHMM supports polarization-sensitive transmission coefficients and thereby achieves micrometer-scale δ, which corresponds to several wavelengths, in spite of the deep-subwavelength total thickness. Shift enhancement, which is defined as δ in vHMM divided by δ in hHMM ($\delta_{vHMM}/\delta_{hHMM}$), proves significant enhancement in a broad range. The shift enhancement, which depends on θ_i, shows extreme enhancement at small θ_i and, therefore, can be further increased by decreasing it (Figure 3g). δ is 800-fold enhanced when $\theta_i = 5°$ (Figure 3f) and 5000-fold enhanced when $\theta_i = 1°$ (see shift and shift enhancement at small incident angle, Supporting Information). We would like to emphasize that although we use Ag and TiO_2 for quantitative demonstration, the enhancement of OSHE in vHMM is true in general, and is not limited to the specific combination of materials.

While hHMMs can be fabricated readily by repetition of thin film evaporation, fabrication of vHMM is challenging because of high aspect ratio and difficulty in filling the vacancies. Therefore, we propose a gold nanograting on a glass substrate as a realistic structure (Figure 4a). Here, air (n = 1) corresponds to the dielectric part, and the effective medium consisting of gold and air with f = 0.5 possesses type-II hyperbolic dispersion (see effective permittivities and dispersion of a vertical hyperbolic metamaterial consisting of gold and air, Supporting Information). The geometrical parameters are taken as width w = 110 nm, period $p = 2w$, and height h = 50 nm. Despite the thickness of a few tens of nanometers, such grating structures have shown hyperbolic dispersion and related phenomena, such as negative refraction and diffraction-unlimited propagation of surface waves.[21−23]

Transmission coefficients of the gold nanograting are calculated using COMSOL Multiphysics (crossmarkers in Figure 4b,c). Transmission coefficients when w = 5 nm and those calculated by EMT are plotted as references. Then we

DOI: 10.1021/acsphotonics.9b00904
ACS Photonics 2019, 6, 2530−2536

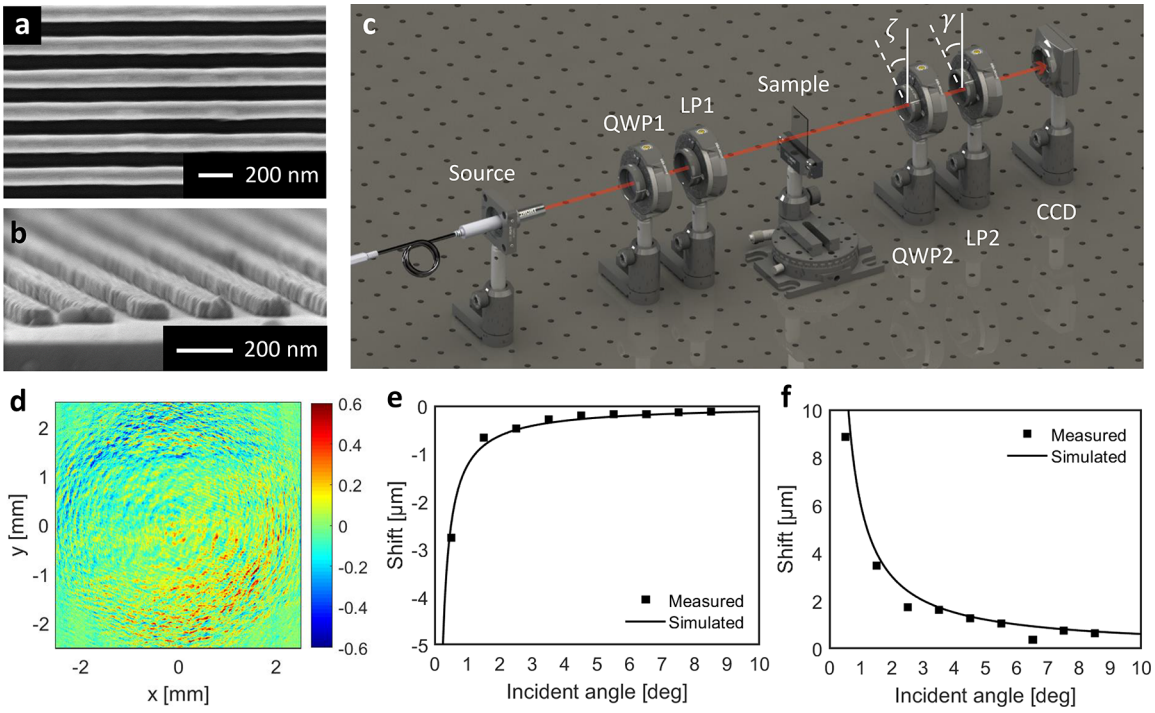

Figure 5. (a) Top view and (b) perspective view of the fabricated sample obtained by scanning electron microscopy. (c) Schematics of Stokes polarimetry setup. (d) Experimentally measured s_3 distribution at 532 nm when the incident angle is 5.5°. Simulated and measured δ at (e) 532 nm and (f) 638 nm. Error bars are not plotted here as they are smaller than the point marker.

use eq 2 to calculate δ. Since the realistic structure is not sufficiently deep-subwavelength, the spectra and δ disagree slightly with the result obtained using EMT. δ of the realistic structure divided by δ calculated by EMT is shown in Figure 4e. The geometrical discrepancy between the realistic structure and the effective medium model results in disagreement at short wavelength. As the width of the grating becomes comparable to the wavelength, EMT breaks down, and the reflection spectrum of the grating exhibits a broad peak near 600 nm for p-polarization. The high reflection results in a dip in t_p, which is not predicted by EMT. Nevertheless, δ of the realistic structure is still several orders of magnitude higher than that of hHMMs.

Since the transmission coefficients are given, we can calculate field amplitude distribution of a circularly polarized transmitted Gaussian beam by applying the boundary conditions.[8] The field distributions of the transmitted beam at 532 nm are shown in Figure 4f,g. Field amplitude along the white dashed line shows transverse shift of two circularly polarized light. At 532 nm where $\delta < 0$, LCP (RCP) is shifted to the $-y$ ($+y$) direction with $\delta = -0.24$ μm (Figure 4h). On the other hand, at 638 nm where $\delta > 0$, δ is reversed and LCP is shifted by $\delta = 1.22$ μm (Figure 4i).

A centimeter-scale gold nanograting is patterned on a glass substrate by using nanoimprint lithography. Scanning electron microscopy images of the fabricated sample are shown in Figure 5a,b. In order to experimentally demonstrate the OSHE, we use Stokes polarimetry methods,[9,24] which have been proposed to measure δ. Stokes parameters, which characterize the polarization states, are measured in this measurement, and will be used to calculate δ later. Schematics of the setup is shown in Figure 5c. Diode lasers with wavelength 532 and 638 nm are used as sources. The incident Gaussian beam is linearly polarized by 45° after passing the first linear polarizer (LP1). Then the beam passes the sample, a quarter-wave plate and an additional linear polarizer in sequence and then is captured by a position-sensitive CCD camera. The distributions of Stokes parameters of the transmitted beam are[24]

$$\begin{aligned} S_0(\mathbf{R}) &= I(0^\circ, 0^\circ) + I(0^\circ, 90^\circ) \\ S_1(\mathbf{R}) &= I(0^\circ, 0^\circ) - I(0^\circ, 90^\circ) \\ S_2(\mathbf{R}) &= I(0^\circ, 45^\circ) - I(0^\circ, 135^\circ) \\ S_3(\mathbf{R}) &= I(90^\circ, 45^\circ) - I(90^\circ, 135^\circ) \end{aligned} \tag{4}$$

where $I(\zeta,\gamma)$ is the local intensity when retardation angle of the second quarter-wave plate (QWP2) is ζ and rotation angle of the second linear polarizer (LP2) is γ. The normalized third Stokes parameter $s_3(\mathbf{R}) = S_3(\mathbf{R})/S_0(\mathbf{R})$ represents the local ellipticity of the transmitted Gaussian beam (Figure 5d). Different handedness of the ellipticity manifests the helicity-dependent splitting along the y-axis. Red and blue color in Figure 5d correspond to LCP and RCP, respectively. As predicted by Figure 4, LCP (RCP) is shifted to $-y$ ($+y$) direction at 532 nm. Furthermore, δ can be calculated by the measured Stokes parameter using the following formula.[24]

$$\delta = \frac{\cot\theta_i}{k}(-\sigma(1 - \cos\Phi_0) + \chi \sin\Phi_0) \tag{5}$$

Here, $\Phi_0 = \tan^{-1}(\tilde{S}_3/\tilde{S}_2)$, where $\tilde{S}_j$ is the integrated Stokes parameter defined as $\tilde{S}_j = \int S_j(\mathbf{R})d^2\mathbf{R}$, $\sigma = 2\mathrm{Im}(\alpha^*\beta)$ and $\chi = 2\mathrm{Re}(\alpha^*\beta)$, where $(\alpha\ \beta)^T$ is the Jones vector of the incident beam ($\alpha = \beta = 1/\sqrt{2}$). The measured δ at 532 nm (Figure 5e) and at 638 nm (Figure 5f), obtained by eq 5, agree well with the simulation. In 10 consecutive experiments performed with the same θ_i, ζ and γ, the standard deviation of δ is less than 1% of its value. As predicted by eq 2, δ diverges as the incident angle goes to zero. The maximum δ, which is

DOI: 10.1021/acsphotonics.9b00904
ACS Photonics 2019, 6, 2530−2536

approximately 9 μm in our measurement, can be further enhanced significantly by reducing θ_i. The measured transmittance of the sample, which is calculated by the ratio of $\tilde{S}_0$ of the sample to $\tilde{S}_0$ of free space, is 0.44 ± 0.01 at 532 nm and 0.25 at 632 nm. The high efficiency resulting from a deep-subwavelength thin sample will be beneficial in developing spin-dependent photonic devices.

In conclusion, we demonstrate an enhanced optical spin Hall effect in a deep-subwavelength thin vertical hyperbolic metamaterial. A high discrepancy between the effective permittivities experienced by s- and p-polarizations provides the several orders of magnitude enhanced shift compared to that in a horizontal hyperbolic metamaterial. Optical spin Hall effect is experimentally demonstrated by using a gold nanograting via Stokes polarimetry setup. Although period of the grating is not small enough to satisfy effective medium theory in our experiment, the transverse shift of a micrometer-scale is obtained. The optical spin Hall effect of a vertical hyperbolic metamaterial with period much smaller than the wavelength can be demonstrated by scaling down the period by adopting sophisticated fabrication techniques[25] or in terahertz regime using the current technology. The huge optical spin Hall effect in a vertical hyperbolic metamaterial provides a way to realize compact photonic devices with spin degree-of-freedom such as filters, sensors, switches, and beam splitters.

METHODS

Fabrication. Gold nanograting patterns (2 × 2 cm area) having 220 nm period were fabricated by a process based on nanoimprint lithographys. Poly(methyl methacrylate) (PMMA) resist was spin-cast on a glass substrate, then imprinted using a SiO_2 mold (50 bar and 170 °C for 7 min) and demolded after cooling it down to room temperature. Chromium (Cr) was selectively deposited on each sidewall of the imprinted nanograting structure by angled deposition. The Cr, deposited on the patterns, induced development of an undercut structure during O_2 reactive ion etching (RIE). This process facilitated the lift-off process and controlled the linewidth of the resultant metal grating. O_2 RIE was performed using 10 sccm of O_2 at chamber pressure of 40 mTorr and bias power of 40 W. Ti (2 nm) and gold (50 nm) were deposited using an E-beam evaporator, and the lift-off process provided gold nanograting patterns. A 2 nm thick Ti seed layer was used to improve the adhesion of the following gold layer.

Stokes Polarimetry Measurement. A polarimetric technique was used to measure the shifts of the beam transmitted through the vHMM. We employed two diode lasers, one with a wavelength λ = 638 nm (Thorlabs, L638P040) and one with λ = 532 nm (Thorlabs, CPS532). The beam was linearly polarized after a Glan-Tompson polarizer (Thorlabs, GL15) and illuminated to the vHMM at various tilted angles. The beam was captured by a CCD camera (Thorlabs, DCC1545M) after passing through a quarter-wave plate (Thorlabs, AQWP10M-580) and another Glan-Tompson polarizer.

ASSOCIATED CONTENT

Supporting Information

The Supporting Information is available free of charge on the ACS Publications website at DOI: 10.1021/acsphotonics.9b00904.

Detailed theory of transmission coefficients from effective medium theory, effective permittivities and dispersion of a vertical hyperbolic metamaterial consisting of gold and air, optical spin Hall effect in a type-i hyperbolic metamaterial, shift and shift enhancement at small incident angle, comparison between vertically- and horizontally-stacked dielectric multilayers, and effect of diffraction in the measurement (PDF)

AUTHOR INFORMATION

Corresponding Author

*E-mail: jsrho@postech.ac.kr.

ORCID

Hui Joon Park: 0000-0003-4607-207X

Junsuk Rho: 0000-0002-2179-2890

Author Contributions

‡These authors contributed equally to this work.

Notes

The authors declare no competing financial interest.

ACKNOWLEDGMENTS

This work was financially supported by the National Research Foundation of Korea (NRF) Grants (NRF-2019R1A2C3003129, CAMM-2019M3A6B3030637, NRF-2019R1A5A8080290, NRF-2018M3D1A1058998, NRF-2015R1A5A1037668) funded by the Ministry of Science and ICT (MSIT) of the Korean government. M.K. acknowledges Global Ph.D. Fellowship (NRF-2017H1A2A1043204) from NRF-MSIT of the Korean government.

REFERENCES

(1) Jacob, Z.; Alekseyev, L. V.; Narimanov, E. Optical Hyperlens: Far-field imaging beyond the diffraction limit. *Opt. Express* **2006**, *14*, 8247−8256.

(2) Rho, J.; Ye, Z.; Xiong, Y.; Yin, X.; Liu, Z.; Choi, H.; Bartal, G.; Zhang, X. Spherical hyperlens for two-dimensional sub-diffractional imaging at visible frequencies. *Nat. Commun.* **2010**, *1*, 143.

(3) Lee, D.; Kim, Y. D.; Kim, M.; So, S.; Choi, H.-J.; Mun, J.; Nguyen, D. M.; Badloe, T.; Ok, J. G.; Kim, K.; Lee, H.; Rho, J. Realization of Wafer-Scale Hyperlens Device for Sub-diffractional Biomolecular Imaging. *ACS Photonics* **2018**, *5*, 2549−2554.

(4) Byun, M.; Lee, D.; Kim, M.; Kim, Y.; Kim, K.; Ok, J. G.; Rho, J.; Lee, H. Demonstration of nanoimprinted hyperlens array for high-throughput sub-diffraction imaging. *Sci. Rep.* **2017**, *7*, 46314.

(5) Jacob, Z.; Kim, J.-Y.; Naik, G. V.; Boltasseva, A.; Narimanov, E. E.; Shalaev, V. M. Engineering photonic density of states using metamaterials. *Appl. Phys. B: Lasers Opt.* **2010**, *100*, 215−218.

(6) Yang, X.; Yao, J.; Rho, J.; Yin, X.; Zhang, X. Experimental realization of three-dimensional indefinite cavities at the nanoscale with anomalous scaling laws. *Nat. Photonics* **2012**, *6*, 450.

(7) Tang, T.; Zhang, Y.; Li, J.; Luo, L. Spin Hall Effect Enhancement of Transmitted Light Through an Anisotropic Metamaterial Slab. *IEEE Photonics J.* **2017**, *9*, 1−10.

(8) Tang, T.; Li, C.; Luo, L. Enhanced spin Hall effect of tunneling light in hyperbolic metamaterial waveguide. *Sci. Rep.* **2016**, *6*, 30762.

(9) Takayama, O.; Sukham, J.; Malureanu, R.; Lavrinenko, A. V.; Puentes, G. Photonic spin Hall effect in hyperbolic metamaterials at visible wavelengths. *Opt. Lett.* **2018**, *43*, 4602−4605.

(10) Onoda, M.; Murakami, S.; Nagaosa, N. Hall Effect of Light. *Phys. Rev. Lett.* **2004**, *93*, 083901.

(11) Bliokh, K. Y.; Bliokh, Y. P. Conservation of Angular Momentum, Transverse Shift, and Spin Hall Effect in Reflection and Refraction of an Electromagnetic Wave Packet. *Phys. Rev. Lett.* **2006**, *96*, 073903.

DOI: 10.1021/acsphotonics.9b00904
ACS Photonics 2019, 6, 2530−2536

(12) Yin, X.; Ye, Z.; Rho, J.; Wang, Y.; Zhang, X. Photonic Spin Hall Effect at Metasurfaces. *Science* **2013**, *339*, 1405−1407.
(13) Sun, J.; Shalaev, M. I.; Litchinitser, N. M. Experimental demonstration of a non-resonant hyperlens in the visible spectral range. *Nat. Commun.* **2015**, *6*, 7201.
(14) Bliokh, K. Y.; Aiello, A. Goos−Hnchen and Imbert−Fedorov beam shifts: an overview. *J. Opt.* **2013**, *15*, 014001.
(15) Hosten, O.; Kwiat, P. Observation of the Spin Hall Effect of Light via Weak Measurements. *Science* **2008**, *319*, 787−790.
(16) Zhou, X.; Xiao, Z.; Luo, H.; Wen, S. Experimental observation of the spin Hall effect of light on a nanometal film via weak measurements. *Phys. Rev. A: At., Mol., Opt. Phys.* **2012**, *85*, 043809.
(17) Zhu, W.; She, W. Enhanced spin Hall effect of transmitted light through a thin epsilon-near-zero slab. *Opt. Lett.* **2015**, *40*, 2961−2964.
(18) Zhang, W.; Wu, W.; Chen, S.; Zhang, J.; Ling, X.; Shu, W.; Luo, H.; Wen, S. Photonic spin Hall effect on the surface of anisotropic two-dimensional atomic crystals. *Photonics Res.* **2018**, *6*, 511−516.
(19) Zhou, X.; Ling, X.; Zhang, Z.; Luo, H.; Wen, S. Observation of spin Hall effect in photon tunneling via weak measurements. *Sci. Rep.* **2015**, *4*, 7388.
(20) Agranovich, V.; Kravtsov, V. Notes on crystal optics of superlattices. *Solid State Commun.* **1985**, *55*, 85−90.
(21) Fan, X.; Wang, G. P.; Lee, J. C. W.; Chan, C. T. All-Angle Broadband Negative Refraction of Metal Waveguide Arrays in the Visible Range: Theoretical Analysis and Numerical Demonstration. *Phys. Rev. Lett.* **2006**, *97*, 073901.
(22) Liu, Y.; Zhang, X. Metasurfaces for manipulating surface plasmons. *Appl. Phys. Lett.* **2013**, *103*, 141101.
(23) High, A. A.; Devlin, R. C.; Dibos, A.; Polking, M.; Wild, D. S.; Perczel, J.; de Leon, N. P.; Lukin, M. D.; Park, H. Visible-frequency hyperbolic metasurface. *Nature* **2015**, *522*, 192.
(24) Bliokh, K. Y.; Samlan, C. T.; Prajapati, C.; Puentes, G.; Viswanathan, N. K.; Nori, F. Spin-Hall effect and circular birefringence of a uniaxial crystal plate. *Optica* **2016**, *3*, 1039−1047.
(25) Meng, L.; Gao, J.; He, X.; Li, J.; Wei, Y.; Yan, J. CMOS-Compatible Top-Down Fabrication of Periodic SiO_2 Nanostructures Using a Single Mask. *Nanoscale Res. Lett.* **2015**, *10*, 341.

DOI: 10.1021/acsphotonics.9b00904
ACS Photonics 2019, 6, 2530−2536